

# Hilbert Space Black Hole Analog: Unidirectional Transport without Driving

Elvira Bilokon<sup>1,2,\*</sup>, Valeriia Bilokon<sup>1,2,†</sup>, Frank Großmann<sup>3</sup>, Jason R. Williams<sup>4</sup>, and Denys I. Bondar<sup>1,‡</sup>

<sup>1</sup>*Department of Physics and Engineering Physics,*

*Tulane University, New Orleans, Louisiana 70118, United States*

<sup>2</sup>*Akhiezer Institute for Theoretical Physics, NSC KIPT, Akademichna 1, 61108 Kharkiv, Ukraine*

<sup>3</sup>*Institut für Theoretische Physik, Technische Universität Dresden, D-01062 Dresden, Germany*

<sup>4</sup>*Jet Propulsion Laboratory, California Institute of Technology, Pasadena, CA 91109, USA*

Black holes permit matter to cross their event horizon in only one direction. We show that interacting bosons in optical lattices with asymmetric barrier exhibit an analogous phenomenon, creating unidirectional quantum transport without external driving or dissipation. This directionality emerges purely from many-body interactions, which cause asymmetric projection of the initial state onto transport-enabled or transport-forbidden sectors. The resulting dynamics create an effective one-way boundary in Hilbert space, forming a quantum analog of a black-hole event horizon. Our results establish interactions as a fundamentally new route to directional transport, enabling coherent rectification in atomtronic circuits by the use of intrinsic properties of the system only.

*Introduction*—Astrophysical black holes permit matter to flow in one direction only—an extreme manifestation of broken transport symmetry, where particles cross an event horizon but cannot return. Black hole analogs have been created in systems ranging from acoustic horizons in Bose-Einstein condensates [1–6] to optical event horizons in nonlinear media [7, 8], water wave analogs [9–13], superconductor and superfluid interfaces [14, 15], and lattice models in superconducting qubits [16] where effective metric descriptions mimic gravitational spacetime curvature. While gravity provides the most dramatic realization of such irreversibility, the broader question of how transport acquires a preferred direction extends across physics, from electronic devices to quantum matter.

Directional transport is conventionally achieved through ratchet mechanisms, nonlinear response, or time-dependent driving [17–21]. In quantum systems, directionality has been demonstrated using dissipation [22], coupling to external reservoirs [23], periodic modulation [24, 25], or topological mechanisms [26, 27]. These approaches—whether classical or quantum—predominantly operate at the single-particle level, relying on either explicit time-reversal symmetry breaking through dissipation or engineered time-dependent potentials [25, 28, 29]. The emergence of directional transport in closed, undriven quantum systems has remained an outstanding challenge. This raises a natural question: is there a fundamentally different route to directionality, one that does not rely on driving, dissipation, or reservoirs?

Interactions fundamentally alter this picture. While many-body effects are often associated with transport suppression through self-trapping [30–34] or many-body localization [35–38], interactions can also enable qualitatively new transport phenomena [39, 40]. In systems

combining spatial asymmetry with strong correlations, interactions restructure the accessible eigenstate manifold, potentially creating transport pathways unavailable to single particles. Previous studies of interaction-assisted tunneling [41] and correlated transport in optical lattices [42, 43] have hinted at this possibility, but robust unidirectional transport in static, closed quantum systems has not been demonstrated.

In the autonomous, single particle case, tunneling probabilities are known to be symmetric (i. e. transmission as well as reflection probabilities at a fixed energy are the same from left to right and from right to left) even for asymmetric potentials, as proven [44–46]. In this study, we show that interacting bosons in a one-dimensional optical lattice with a static asymmetric barrier can exhibit one-way quantum transport, however: particles tunnel readily when incident from one direction while remaining trapped from the opposite direction. This behavior emerges entirely from the interplay between barrier asymmetry and many-body interactions, without time-dependent driving, dissipation, or coupling to external reservoirs. Through eigenstate analysis, we reveal that the asymmetric potential selectively projects initial states onto manifolds with fundamentally different transport properties, creating a dynamical horizon in Hilbert space—a quantum analog of the black-hole event horizon. Unlike previous black hole analogs that simulate metric effects in physical space, this Hilbert space horizon arises from interaction-driven eigenstate selection rather than spacetime geometry. Our results have direct implications for atomtronic circuit elements [47, 48], quantum state preparation [49, 50] in optical lattices, and the design of interaction-controlled quantum devices that exploit many-body effects rather than external driving or dissipation.

*Model and Methods*—In our theoretical framework, we investigate the quantum dynamics of ultracold bosons confined to a one-dimensional optical lattice of  $L$  sites,

\* ebilokon@tulane.edu

† vbilokon@tulane.edu

‡ dbondar@tulane.edu

described by the Bose-Hubbard Hamiltonian

$$\hat{\mathcal{H}} = -J \sum_{j=1}^{L-1} \left( \hat{b}_j^\dagger \hat{b}_{j+1} + \hat{b}_{j+1}^\dagger \hat{b}_j \right) + \frac{U}{2} \sum_{j=1}^L \hat{n}_j (\hat{n}_j - 1) + \sum_{j=1}^L V_j^{\text{ex}} \hat{n}_j. \quad (1)$$

Here, the operator  $\hat{b}_j^\dagger$  ( $\hat{b}_j$ ) creates (annihilates) a boson at lattice site  $j$ , satisfying the canonical commutation relations  $[\hat{b}_i, \hat{b}_j^\dagger] = \delta_{ij}$ . The number operator is defined as  $\hat{n}_j = \hat{b}_j^\dagger \hat{b}_j$ . The first term in Eq. (1) represents the kinetic energy arising from the tunneling of bosons between neighboring sites with amplitude  $J$ . The second term describes the on-site repulsive interaction with strength  $U$ , while the final term incorporates a site-dependent external potential  $V_j^{\text{ex}}$ , which can be engineered to create specific trapping geometries. In our study, we consider two configurations of the barrier:

$$V_j^{\text{ex (a)}} = h\delta_{j,L/2} + \frac{h}{2}\delta_{j,L/2+1}, \quad (2)$$

$$V_j^{\text{ex (b)}} = \frac{h}{2}\delta_{j,L/2} + h\delta_{j,L/2+1}, \quad (3)$$

where  $h$  denotes the barrier height and  $\delta_{j,k}$  is the Kronecker delta function (see Fig. 1). For convenience, we denote the Hamiltonian with the barrier defined in Eq. (2) and Eq. (3) as  $\mathcal{H}_a$  and  $\mathcal{H}_b$ , respectively. Configuration in Eq. (2) places the higher barrier at site  $L/2$ , whereas configuration in Eq. (3) places it at site  $L/2 + 1$ , allowing us to study the directional dependence of quantum transport through asymmetric barriers. We mention explicitly that in the above Hamiltonian, we use open boundary conditions.

To prepare the initial quantum state, we employ a two-step protocol that ensures the bosons are initially localized away from the barrier region [see Fig. 1]. First, we introduce a cooling barrier configuration where all sites experience a strong confining potential of height  $3h$ , except for the pre-barrier sites (sites 1 through  $L/2 - 1$ ) which remain at zero potential. This creates an effective trapping region in the left half of the lattice. For example for  $L = 6$ , this localizes bosons on sites 1 and 2, with sites 3–6 experiencing the  $3h$  barrier, creating an effective trapping region in the left half of the lattice. We then obtain the ground state of the system under this cooling barrier configuration. In the second step, we perform a quantum quench by instantaneously switching from the cooling barrier to the asymmetric triangular barrier configuration given by Eqs. (2) or (3). When particles are initialized from the left (pre-barrier region), configuration in Fig. 1(a) corresponds to tunneling from the “vertical side” (encountering height  $h$  first, then  $h/2$ ), while configuration in Fig. 1(b) corresponds to the “angled side” (encountering  $h/2$  first, then  $h$ ). This preparation protocol ensures that all bosons initially reside on one side of the barrier, allowing us to study the subsequent tunneling

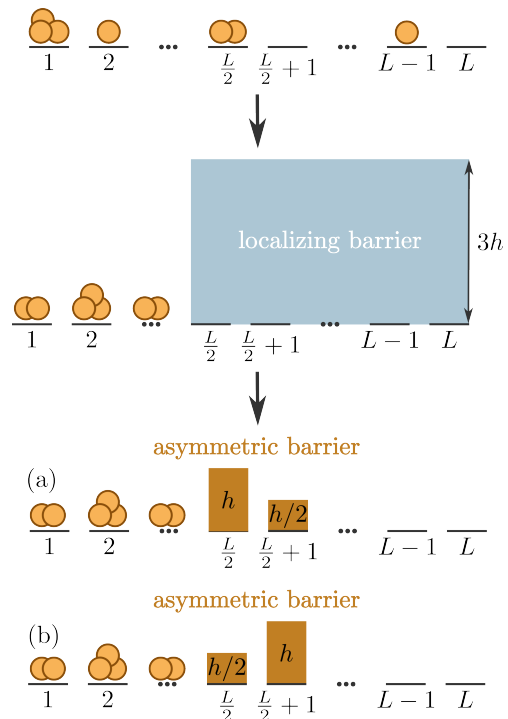


FIG. 1. Initial state preparation protocol. Starting from a random distribution of  $N$  bosons across the  $L$ -site lattice (top), a strong localizing potential ( $3h$ , shown in blue) is applied to all sites except the leftmost  $L/2 - 1$  sites to obtain the ground state (middle). The system is then evolved under the asymmetric triangular barrier configurations: (a) “vertical” orientation with barrier heights  $h$  and  $h/2$  at sites  $L/2$  and  $L/2 + 1$ , respectively, or (b) “angled” orientation with the barrier heights reversed.

dynamics and the emergence of the directional transport phenomena.

The key observable for characterizing directional transport is the population imbalance

$$\Delta n(t) = n_{\text{after}}^{(a)}(t) - n_{\text{after}}^{(b)}(t), \quad (4)$$

where  $n_{\text{after}}^{(k)}(t) = \sum_{j=L/2+2}^L \langle \hat{n}_j \rangle$  measures the particle number in the post-barrier region for configuration  $k \in \{a, b\}$ .

The quantum dynamics are computed using the QuSpin package [51, 52], which provides exact diagonalization and time evolution capabilities for quantum many-body systems. The exact diagonalization approach allows us to fully resolve the quantum many-body dynamics without approximation, capturing all correlation effects and entanglement generation during the tunneling process.

*Discussion*— We start our discussion by characterizing the interaction-driven directional transport in the asymmetric triangular barrier system. For a lattice of  $L = 6$  sites with  $N = 4$  bosons, we fix  $h = 10J$  and systematically vary the interaction strength  $U$  to map out the parameter regime where unidirectional tunneling emerges.

This system size is chosen to balance computational

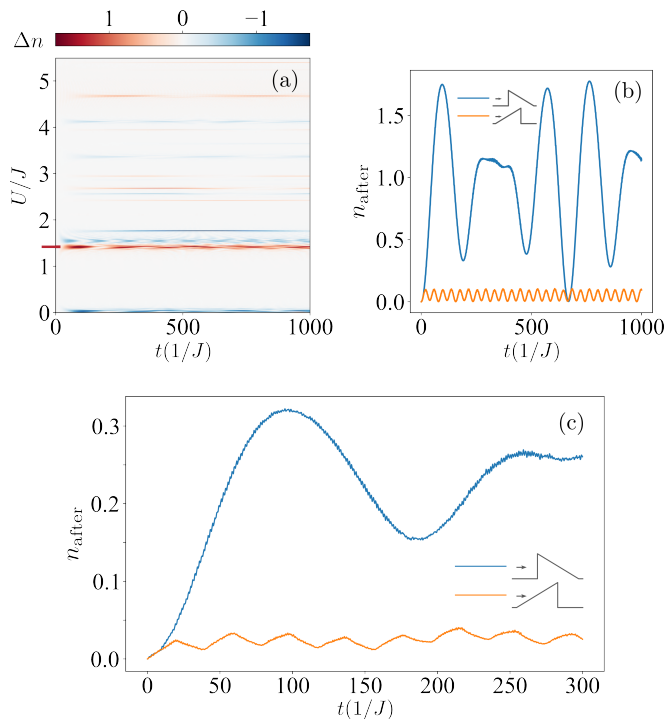


FIG. 2. Directional transport in the asymmetric Bose-Hubbard model. (a) Heatmap showing the population imbalance  $\Delta n$  as a function of interaction strength  $U$  and time  $t$  for  $N = 4$  bosons,  $L = 6$  sites, barrier height  $h = 10J$ , and open boundary conditions. Red (blue) regions indicate preferential tunneling from the vertical (angled) side. The strongest directional transport occurs at  $U \approx 1.42J$  (dark red band). Time evolution of  $n_{\text{after}}$  for  $U = 1.42J$  in case of (b) Fock state and (c) coherent state initial conditions. Blue curve: tunneling from vertical side, indicating collective many-body transport. Orange curve: tunneling from angled side remains suppressed.

tractability with the emergence of many-body effects: the system is small enough to permit exact diagonalization of the full Hilbert space, yet large enough to capture interaction-driven collective dynamics. The filling fraction  $N/L = 2/3$  ensures an average occupation of approximately 2 bosons per site in the pre-barrier region, thereby avoiding self-trapping effects that would suppress tunneling at higher occupations. While the choice of  $h$  is made for concreteness, the unidirectional transport phenomena we describe are not restricted to this particular barrier height and persist across a range of  $h$  values.

Figure 2(a) demonstrates the population imbalance  $\Delta n$  as a function of time  $t$  and interaction strength  $U$ . The heatmap reveals interaction windows with strong directional transport, where particles tunnel readily from one side of the barrier but remain trapped from the other side. The strongest directional asymmetry occurs at  $U \approx 1.42J$ , where positive  $\Delta n$  indicates particles tunnel from the vertical configuration but not from the angled configuration. We focus our analysis on this regime, which exhibits robust directional transport over an extended

parameter range ( $\Delta U \sim 0.05J$ , corresponding to 3.5% relative uncertainty in  $U$ ). Narrower resonance-like features visible at higher  $U$  values are excluded from detailed analysis due to their sensitivity to parameter variations. The required precision  $\delta U/U = 3.5\%$  is readily achievable via Feshbach resonance control within current experimental capabilities [53, 54]. Figure 2(b) demonstrates the directional asymmetry at the interaction strength  $U = 1.42J$ : particles tunnel from the vertical side with large-amplitude oscillations, while the angled configuration exhibits nearly complete suppression of tunneling, with population to the right of the barrier remaining below 0.1 particles throughout the evolution. This dramatic contrast exemplifies the unidirectional transport regime where the interplay between asymmetric barriers and interactions creates effective one-way transport. To emphasize the robustness of the effect, we numerically studied the quantum dynamics for coherent state initial conditions  $|n_1, \dots, n_L\rangle = \prod_{j=1}^L \exp(-n_j^2/2 + \sqrt{n_j} \hat{b}_j^\dagger) |\mathbf{0}\rangle$  where only  $n_1, \dots, n_{L/2-1}$  are nonzero, i.e., for an initial wavefunction that is a direct product of a Poisson distribution over number (Fock) states in each well to the left of the barriers. This initial state is the closest quantum analog to a classical phase-space point as well as an excellent approximation to Bose-Einstein condensates prepared on single particle modes [55]. The quantum dynamics was solved for by using a fully variational approach based on a multi-configuration ansatz in terms of Glauber coherent states [56] (for an implementation of the same initial states but using generalized coherent states as basis functions, see [57]). For the same model parameters as the ones used in Fig. 2 and for  $n_1 = n_2 = 2$  as well as  $n_3, \dots, n_6 = 0$  initially, we find qualitatively similar behavior, although the amplitude of the oscillation in the vertical case is suppressed, as depicted in Fig. 2(c). The stark difference between the tunneling in the vertical and angled configurations is still present, however.

To understand the microscopic mechanism underlying this macroscopic directional transport, we examine the overlap between the initial state  $|\psi_0\rangle$  (the ground state of the system with cooling barrier configuration) and the eigenstates of the Hamiltonians  $\mathcal{H}_a$  and  $\mathcal{H}_b$ . Figure 3 reveals the distinct eigenstate structure underlying the directional tunneling asymmetry. The main panel displays the overlap  $|\langle \psi_i | \psi_0 \rangle|^2$  between the prepared initial state and the eigenstates of the Hamiltonians for both barrier configurations. For particles initially positioned from the angled side (orange curve), the dynamics are dominated by a single eigenstate ( $i = 3$ ) with overlap approaching 0.9, indicating near-perfect projection onto the single state. In stark contrast, initial localization from the vertical side (blue) exhibits fragmented overlap across multiple eigenstates ( $i = 5, 6, 7$ ) with maximum overlap  $\approx 0.4$  signaling a superposition that drives the observed transport. The insets display the Fock-state composition  $|c_j|^2$  of the dominant contributing eigenstates (with the top five Fock-state contributions de-

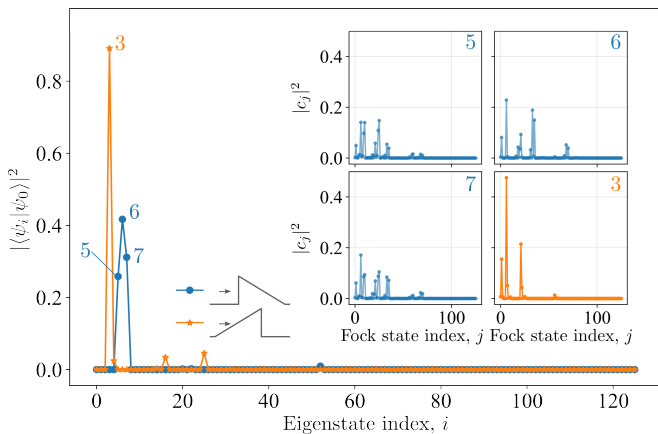


FIG. 3. Eigenstate structure underlying directional transport at  $U = 1.42J$  and  $h = 10J$  for a system of size  $L = 6$  with  $N = 4$  bosons. Main panel: Overlap  $|\langle\psi_i|\psi_0\rangle|^2$  between the prepared initial state (ground state of the system with cooling barrier) and eigenstates of  $\mathcal{H}_a$  (blue) and  $\mathcal{H}_b$  (orange). Initial localization from the angled side projects almost entirely onto a single eigenstate ( $i = 3$ , overlap  $\approx 0.9$ ), while localization from the vertical side creates a superposition of three eigenstates ( $i = 5, 6, 7$ , maximum overlap  $\approx 0.4$ ). Insets: Fock-state composition  $|c_j|^2$  of the dominant eigenstates. The top five Fock-state contributions to these eigenstates are detailed in Table I.

TABLE I. Dominant Fock-state contributions to eigenstates with largest initial state overlap for  $N = 4$  bosons on  $L = 6$  sites at  $U = 1.42J$ ,  $h = 10J$ . Site notation:  $|n_1n_2n_3n_4n_5n_6\rangle$ .

Eigenstate	Fock State	Index $j$	$ c_j ^2$
3 (Angled)	$ 220000\rangle$	6	0.476
	$ 130000\rangle$	21	0.214
	$ 310000\rangle$	1	0.155
	$ 211000\rangle$	7	0.051
	$ 121000\rangle$	22	0.044
5 (Vertical)	$ 120001\rangle$	25	0.147
	$ 220000\rangle$	6	0.141
	$ 210001\rangle$	10	0.140
	$ 120010\rangle$	24	0.109
	$ 210010\rangle$	9	0.097
6 (Vertical)	$ 220000\rangle$	6	0.228
	$ 110020\rangle$	33	0.189
	$ 110002\rangle$	35	0.149
	$ 130000\rangle$	21	0.093
	$ 310000\rangle$	1	0.081
7 (Vertical)	$ 220000\rangle$	6	0.171
	$ 120001\rangle$	25	0.105
	$ 210001\rangle$	10	0.094
	$ 120010\rangle$	24	0.088
	$ 210010\rangle$	9	0.086

tailed in Table I). Crucially, the angled-side eigenstate (bottom right) comprises Fock states with zero post-barrier occupation, creating an effective transport barrier. The vertical-side eigenstates (top panels, bottom left), however, contain substantial weight on configurations with particles distributed across the barrier, en-

abling tunneling. This eigenstate analysis directly connects the macroscopic directional asymmetry to the microscopic many-body structure: the asymmetric barrier geometry selects fundamentally different superpositions of Fock states, yielding opposite transport behaviors despite identical interaction strengths.

*Conclusions*—We have demonstrated that interacting bosons in an optical lattice with an asymmetric barrier exhibit robust unidirectional quantum transport without external driving, dissipation, or coupling to reservoirs. This directionality emerges solely from the interplay between barrier geometry and many-body interactions, establishing a new route to transport rectification in closed quantum systems. The observed directionality is present for Fock state as well as for coherent state initial conditions and for a broad range of system parameters.

Eigenstate analysis reveals the mechanism: the asymmetric barrier projects initial states onto manifolds with opposite transport properties. From one direction, the system projects onto eigenstates comprising Fock states with zero post-barrier occupation, forbidding transport. From the opposite direction, it projects onto eigenstates with significant post-barrier occupation, enabling transport. This creates an effectively one-way dynamical boundary in Hilbert space—a quantum analog of a black hole event horizon.

The interaction-driven mechanism persists across varying particle numbers and system sizes, with experimental precision readily achievable via Feshbach resonance control. Our results identify interactions as an intrinsic mechanism for directionality and open new possibilities for atomtronic devices and coherent many-body transport control.

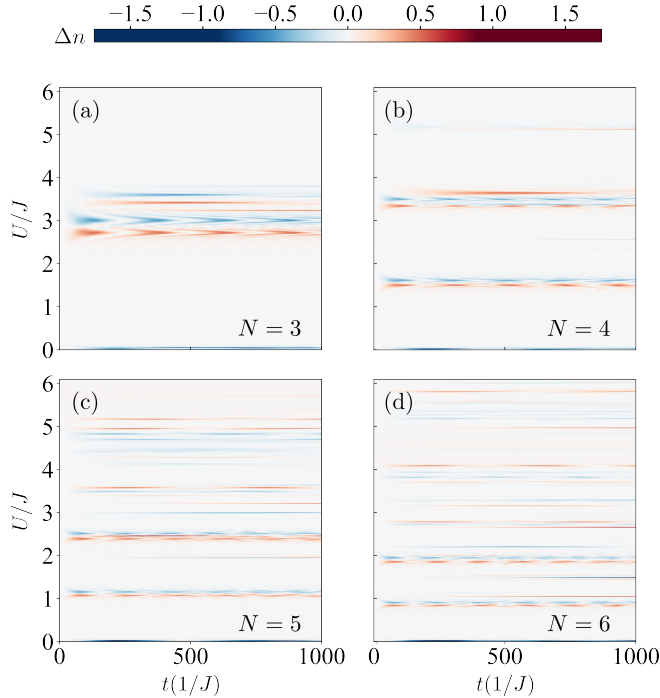
*Acknowledgments.* E.B. was supported by the National Science Foundation (NSF) IMPRESS-U Grant No. 2403609. D.I.B. was supported by Army Research Office (ARO) (grant W911NF-23-1-0288; program manager Dr. James Joseph). The views and conclusions contained in this document are those of the authors and should not be interpreted as representing the official policies, either expressed or implied, of ARO, NSF, or the U.S. Government. The U.S. Government is authorized to reproduce and distribute reprints for Government purposes notwithstanding any copyright notation herein.

- 
- [1] L. J. Garay, J. R. Anglin, J. I. Cirac, and P. Zoller, *Phys. Rev. Lett.* **85**, 4643 (2000).
- [2] R. Balbinot, A. Fabbri, S. Fagnocchi, A. Recati, and I. Carusotto, *Phys. Rev. A* **78**, 021603 (2008).
- [3] I. Carusotto, S. Fagnocchi, A. Recati, R. Balbinot, and A. Fabbri, *New Journal of Physics* **10**, 103001 (2008).
- [4] J. Macher and R. Parentani, *Phys. Rev. A* **80**, 043601 (2009).
- [5] O. Lahav, A. Itah, A. Blumkin, C. Gordon, S. Rinott, A. Zayats, and J. Steinhauer, *Phys. Rev. Lett.* **105**, 240401 (2010).
- [6] J. Steinhauer, *Nature Physics* **12**, 959 (2016).
- [7] T. G. Philbin, C. Kuklewicz, S. Robertson, S. Hill, F. König, and U. Leonhardt, *Science* **319**, 1367 (2008).
- [8] M. Elazar, V. Fleurov, and S. Bar-Ad, *Phys. Rev. A* **86**, 063821 (2012).
- [9] G. Rousseaux, C. Mathis, P. Maïssa, T. G. Philbin, and U. Leonhardt, *New Journal of Physics* **10**, 053015 (2008).
- [10] S. Weinfurter, E. W. Tedford, M. C. J. Penrice, W. G. Unruh, and G. A. Lawrence, *Phys. Rev. Lett.* **106**, 021302 (2011).
- [11] L.-P. Euvé, F. Michel, R. Parentani, T. G. Philbin, and G. Rousseaux, *Phys. Rev. Lett.* **117**, 121301 (2016).
- [12] L.-P. Euvé, S. Robertson, N. James, A. Fabbri, and G. Rousseaux, *Phys. Rev. Lett.* **124**, 141101 (2020).
- [13] G. G. Rozenman, F. Ullinger, M. Zimmermann, M. A. Efremov, L. Shemer, W. P. Schleich, and A. Arie, *Communications Physics* **7**, 165 (2024).
- [14] S. K. Manikandan and A. N. Jordan, *Phys. Rev. D* **96**, 124011 (2017).
- [15] S. K. Manikandan and A. N. Jordan, *Phys. Rev. D* **98**, 124043 (2018).
- [16] Y.-H. Shi, R.-Q. Yang, Z. Xiang, Z.-Y. Ge, H. Li, Y.-Y. Wang, K. Huang, Y. Tian, X. Song, D. Zheng, K. Xu, R.-G. Cai, and H. Fan, *Nature Communications* **14**, 3263 (2023).
- [17] P. Hänggi and F. Marchesoni, *Rev. Mod. Phys.* **81**, 387 (2009).
- [18] J. Rousselet, L. Salome, A. Ajdari, and J. Prost, *Nature* **370**, 446 (1994).
- [19] R. D. Astumian and P. Hänggi, *Physics Today* **55**, 33 (2002).
- [20] P. Reimann, *Physics Reports* **361**, 57 (2002).
- [21] H. Linke, T. E. Humphrey, A. Löfgren, A. O. Sushkov, R. Newbury, R. P. Taylor, and P. Omling, *Science* **286**, 2314 (1999).
- [22] C. Mennerat-Robilliard, D. Lucas, S. Guibal, J. Tabosa, C. Jurczak, J.-Y. Courtois, and G. Grynberg, *Phys. Rev. Lett.* **82**, 851 (1999).
- [23] D. Sánchez and M. Büttiker, *Phys. Rev. Lett.* **93**, 106802 (2004).
- [24] H. Lignier, C. Sias, D. Ciampini, Y. Singh, A. Zenesini, O. Morsch, and E. Arimondo, *Phys. Rev. Lett.* **99**, 220403 (2007).
- [25] S. Denisov, S. Flach, and P. Hänggi, *Physics Reports* **538**, 77 (2014).
- [26] M. Lohse, C. Schweizer, O. Zilberberg, M. Aidelsburger, and I. Bloch, *Nature Physics* **12**, 350 (2016).
- [27] S. Nakajima, T. Tomita, S. Taie, T. Ichinose, H. Ozawa, L. Wang, M. Troyer, and Y. Takahashi, *Nature Physics* **12**, 296 (2016).
- [28] T. Salger, S. Kling, T. Hecking, C. Geckeler, L. Morales-Molina, and M. Weitz, *Science* **326**, 1241 (2009).
- [29] C. E. Creffield and F. Sols, *Phys. Rev. A* **84**, 023630 (2011).
- [30] A. Smerzi, S. Fantoni, S. Giovanazzi, and S. R. Shenoy, *Phys. Rev. Lett.* **79**, 4950 (1997).
- [31] M. Albiez, R. Gati, J. Fölling, S. Hunsmann, M. Cristiani, and M. K. Oberthaler, *Phys. Rev. Lett.* **95**, 010402 (2005).
- [32] T. Anker, M. Albiez, R. Gati, S. Hunsmann, B. Eiermann, A. Trombettoni, and M. K. Oberthaler, *Phys. Rev. Lett.* **94**, 020403 (2005).
- [33] S. I. Mistakidis, K. Mukherjee, S. M. Reimann, and H. R. Sadeghpour, *Phys. Rev. A* **110**, 013323 (2024).
- [34] A. Alaña, M. Modugno, P. Capuzzi, and D. M. Jezek, *Phys. Rev. A* **111**, L051307 (2025).
- [35] D. Basko, I. Aleiner, and B. Altshuler, *Annals of Physics* **321**, 1126 (2006).
- [36] R. Nandkishore and D. A. Huse, *Annual Review of Condensed Matter Physics* **6**, 15–38 (2015).
- [37] M. Schreiber, S. S. Hodgman, P. Bordia, H. P. Lüschen, M. H. Fischer, R. Vosk, E. Altman, U. Schneider, and I. Bloch, *Science* **349**, 842–845 (2015).
- [38] P. Sierant, M. Lewenstein, A. Scardicchio, L. Vidmar, and J. Zakrzewski, *Reports on Progress in Physics* **88**, 026502 (2025).
- [39] M. Eckstein, M. Kollar, and P. Werner, *Phys. Rev. Lett.* **103**, 056403 (2009).
- [40] E. Bilokon, V. Bilokon, D. R. Lindberg, L. Kaplan, A. Sotnikov, and D. I. Bondar, *Communications Physics* **8**, 259 (2025).
- [41] L. Morales-Molina and S. Flach, *New Journal of Physics* **10**, 013008 (2008).
- [42] J. P. Ronzheimer, M. Schreiber, S. Braun, S. S. Hodgman, S. Langer, I. P. McCulloch, F. Heidrich-Meisner, I. Bloch, and U. Schneider, *Phys. Rev. Lett.* **110**, 205301 (2013).
- [43] E. Haller, R. Hart, M. J. Mark, J. G. Danzl, L. Reichsöllner, and H.-C. Nägerl, *Phys. Rev. Lett.* **104**, 200403 (2010).
- [44] L. D. Landau and E. M. Lifshitz, *Quantum mechanics: non-relativistic theory*, Vol. 3 (Elsevier, 1981).
- [45] D. J. Tannor, *Introduction to Quantum Mechanics : a time-dependent perspective* (Univ. Science Books, 2007).
- [46] M. R. A. Shegelski and C. Sample, *Eur. J. Phys.* **41**, 035405 (2020).
- [47] L. Amico and et al., *AVS Quantum Science* **3**, 039201 (2021).
- [48] L. Amico, D. Anderson, M. Boshier, J.-P. Brantut, L.-C. Kwek, A. Minguzzi, and W. von Klitzing, *Rev. Mod. Phys.* **94**, 041001 (2022).
- [49] Christian Gross and Immanuel Bloch, *Science* **357**, 995 (2017).
- [50] A. M. Kaufman and K.-K. Ni, *Nature Physics* **17**, 1324 (2021).
- [51] P. Weinberg and M. Bukov, *SciPost Phys.* **2**, 003 (2017).
- [52] P. Weinberg and M. Bukov, *SciPost Phys.* **7**, 020 (2019).
- [53] A. Marte, T. Volz, J. Schuster, S. Dürr, G. Rempe, E. G. M. van Kempen, and B. J. Verhaar, *Phys. Rev. Lett.* **89**, 283202 (2002).
- [54] M. Borkowski, L. Reichsöllner, P. Thekkepatt,

- V. Barbé, T. van Roon, K. van Druten, and F. Schreck, Review of Scientific Instruments **94**, 073202 (2023).
- [55] E. H. Lieb, R. Seiringer, and J. Yngvason, Reports on Mathematical Physics **59**, 389 (2007).
- [56] M. Werther and F. Großmann, Phys. Rev. B **101**, 174315 (2020).
- [57] Y. Qiao, F. Großmann, P. Schlagheck, and G. M. Lando, Phys. Rev. Lett. **135**, 060404 (2025).

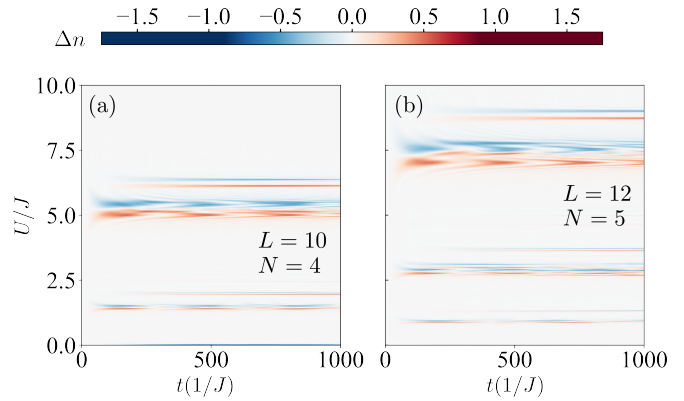
### Supplementary Note 1: DEPENDENCE OF “BLACK-HOLE” REGIME ON PARTICLE NUMBER AND SYSTEM SIZE

In this section we analyze how the “black-hole” region—identified by a large and persistent population imbalance  $\Delta n$ —depends on the total number of bosons in the system and the system size. We begin by examining the particle number dependence for a fixed chain of length  $L = 8$  with barrier height  $h = 10J$ . The total particle number  $N$  is varied as indicated in Fig. 1, specifically  $N = 3, 4, 5, 6$ .



Supplementary Figure 1. Population imbalance  $\Delta n$  as a function of time  $t$  and interaction strength  $U$  for varying particle numbers: (a)  $N = 3$ , (b)  $N = 4$ , (c)  $N = 5$ , and (d)  $N = 6$ . System parameters:  $L = 8$  sites, barrier height  $h = 10J$ , open boundary conditions. Red (blue) regions indicate preferential tunneling from the vertical (angled) side.

For  $N = 3$  particles [see Fig. 1(a)], the system exhibits multiple directional transport regimes within a continuous interaction window  $2.5J \lesssim U \lesssim 3.75J$ . These regimes alternate between favoring tunneling from vertical side (red regions, positive  $\Delta n$ ) and tunneling from angled side (blue regions, negative  $\Delta n$ ), with blue bands typically following red ones. As the particle number increases, the structure of the population imbalance undergoes a qualitative change. At  $N = 4$  [Fig. 1(b)], the single broad region splits into two spatially separated bands centered around  $U \approx 1.5J$  and  $U \approx 3.5J$ . Increasing the filling further to  $N = 5$  [Fig. 1(c)] and  $N = 6$  [Fig. 1(d)] enhances this fragmentation. The splitting reflects the restructuring of the many-body spectrum at higher filling. Adding particles introduces interaction-



Supplementary Figure 2. Population imbalance  $\Delta n$  as a function of time  $t$  and interaction strength  $U$  for: (a)  $L = 10$  and  $N = 4$ , (b)  $L = 12$  and  $N = 5$ ; barrier height  $h = 10J$ , open boundary conditions. Red (blue) regions indicate preferential tunneling from the vertical (angled) side.

assisted tunneling channels and differentially affects the tunneling dynamics for the two barrier configurations.

Having established how particle number affects the transport windows at fixed system size, we now examine how these features scale with the lattice length while maintaining low particle density. Figure 2 shows results for two representative cases:  $L = 10$  sites with  $N = 4$  particles [Fig. 2(a)] and  $L = 12$  sites with  $N = 5$  particles [Fig. 2(b)], both maintaining approximately one boson per site before the barrier. As before, the barrier height is fixed at  $h = 10J$ . Both system sizes exhibit a relatively broad window of large population imbalance. However, with the increase of the system size, the window shifts to higher interaction strengths  $U$ . Within these broad windows, the characteristic alternating pattern persists, with blue regions typically following red regions. Beyond the primary broad window, both systems display additional narrow stripes of large population imbalance at lower interaction strengths. Notably, the larger system exhibits a greater number of such stripes. The persistence of both broad and narrow directional transport windows across system sizes demonstrates that this phenomenon is not a finite-size artifact but rather a fundamental feature of interaction-driven dynamics in asymmetric barriers.

These results have important experimental implications: while the transport effect persists across all particle numbers studied, experiments at lower filling fractions will observe broader, more experimentally accessible parameter windows for directional tunneling.